

An optical-lattice-based quantum simulator for relativistic field theories and topological insulators

This article has been downloaded from IOPscience. Please scroll down to see the full text article.

2012 New J. Phys. 14 015007

(<http://iopscience.iop.org/1367-2630/14/1/015007>)

View [the table of contents for this issue](#), or go to the [journal homepage](#) for more

Download details:

IP Address: 130.183.90.175

The article was downloaded on 21/02/2013 at 10:01

Please note that [terms and conditions apply](#).

An optical-lattice-based quantum simulator for relativistic field theories and topological insulators

Leonardo Mazza^{1,7}, Alejandro Bermudez², Nathan Goldman³,
Matteo Rizzi^{1,4}, Miguel Angel Martin-Delgado⁵ and
Maciej Lewenstein^{4,6}

¹ Max-Planck-Institut für Quantenoptik, D-85748 Garching, Germany

² Institut für Theoretische Physik, Universität Ulm, D-89069 Ulm, Germany

³ Center for Nonlinear Phenomena and Complex Systems—Université Libre de Bruxelles, B-1050 Brussels, Belgium

⁴ Kavli Institute for Theoretical Physics, University of California, Santa Barbara, CA 93106, USA

⁵ Departamento de Física Teórica I, Universidad Complutense, E-28040 Madrid, Spain

⁶ ICFO—Institut de Ciències Fotòniques, E-08860 Castelldefels (Barcelona), Spain and ICREA—Institut Catalana de Recerca i Estudis Avançats, E-08010 Barcelona, Spain

E-mail: leonardo.mazza@mpq.mpg.de

New Journal of Physics **14** (2012) 015007 (27pp)

Received 04 May 2011

Published 31 January 2012

Online at <http://www.njp.org/>

doi:10.1088/1367-2630/14/1/015007

Abstract. We present a proposal for a versatile cold-atom-based quantum simulator of relativistic fermionic theories and topological insulators in arbitrary dimensions. The setup consists of a spin-independent optical lattice that traps a collection of hyperfine states of the same alkaline atom, to which the different degrees of freedom of the field theory to be simulated are then mapped. We show that the combination of bi-chromatic optical lattices with Raman transitions can allow the engineering of a spin-dependent tunneling of the atoms between neighboring lattice sites. These assisted-hopping processes can be employed for the quantum simulation of various interesting models, ranging from non-interacting relativistic fermionic theories to topological insulators. We present a toolbox for the realization of different types of relativistic lattice fermions, which can then be exploited to synthesize a majority of phases in the periodic table of topological insulators.

⁷ Author to whom any correspondence should be addressed.

Contents

1. Introduction	2
2. The setup and the idea	3
3. Realization of spin-dependent hopping operators	7
3.1. Coupling between different hyperfine manifolds	7
3.2. Developing an effective ‘6-level model’	8
3.3. Range of validity of the ‘6-level model’	10
3.4. Diagonal hopping operator	11
3.5. Non-diagonal hopping operator	12
4. From a spin-dependent hopping operator to a quantum simulator	14
5. Applications of the quantum simulator	18
5.1. The zoo of relativistic lattice fermions	18
5.2. A toolbox for topological insulators	21
6. Conclusions	24
Acknowledgments	25
References	25

1. Introduction

In a seminal paper published in 1982 [1], Feynman discussed in great detail the problems connected with the numerical simulation of quantum systems. He envisaged a possible solution, the so-called *universal quantum simulator*, a quantum-mechanical version of the usual simulators and computers currently exploited in many applications of the ‘classical’ world. If realized, such a device would be able to tackle many-body problems with local interactions by using the quantum properties of nature itself [2]. Interestingly, even without the advent of a fully universal quantum computer, the construction of small dedicated devices, also known as *purpose-based quantum simulators*, would already be of significant importance for the understanding of quantum physics. The basic idea is to engineer the Hamiltonian of the quantum model of interest in a highly controllable quantum system and to retrieve all of the desired information with a measurement of its properties. Many research fields would eventually benefit from such devices: for example, two-dimensional (2D) and 3D many-body physics, non-equilibrium dynamics or lattice gauge theories [3].

In recent years, the scientific community has been considering ultra-cold atoms as one of the most promising candidates for the realization of a wide variety of dedicated quantum simulations [4, 5]. Indeed, these gases are genuine quantum systems where the available experimental techniques offer an impressive degree of control together with high-fidelity measurements, thus combining two fundamental requirements for a quantum simulator. Among the most recent experimental achievements, we would like to mention the observation of Anderson localization in disordered Bose–Einstein condensates (BECs) [6, 7], the research on itinerant ferromagnetism with cold fermions [8] or the reconstruction of the equation of state of fermionic matter in extreme conditions, such as in neutron stars [9].

An important drawback in the applicability of cold atoms as quantum simulators is the difficulty of coupling their spatial degrees of freedom to external magnetic fields. This

prevents a direct simulation of quantum Hall physics [10], the controlled observation of whose extraordinary phenomenology would shed new light on quantum many-body theory. One way of overcoming this problem is to dress the system with ingenious laser schemes, which mimic the effect of an external magnetic field, and thus allow the neutral atoms to behave like effectively charged particles [11]. This approach led recently to the realization of neutral BECs coupled to external effective magnetic and electric fields [12, 13], or even with an effective spin–orbit coupling [14]. More generally, the scientific community has realized that even in the presence of an optical lattice, dressing cold gases with suitable optical and microwave transitions could push the experiments beyond the standard superfluid–Mott insulator transition and significantly widen the spectrum of the models that are currently being simulated⁸. Possible applications of such optical-lattice-based quantum simulations are numerous and diverse, ranging from the realization of Abelian and non-Abelian static gauge fields [11, 15–18] to that of quantum Hall states [19–23]; from the study of the anomalous quantum Hall effect [24, 25] to the quantum spin Hall effect [26–28]; from 3D topological insulators [28, 29], to flat-band physics with a non-trivial topological order [30, 31], or non-Abelian anyons [32]. Recently, a great deal of effort has also been put in designing schemes where the exotic effects associated with relativistic quasiparticles, such as Klein tunneling and *Zitterbewegung*, arise in a controlled table-top experiment [33–40].

In this paper, we elaborate on the idea of using a spin-independent bi-chromatic optical lattice dressed with suitable Raman transitions to simulate interesting non-interacting field theories of lattice fermions. We present a concrete proposal to create a 3D optical lattice that traps a multi-species atomic gas and to tailor arbitrary spin-dependent hopping operators. We have already shown how this setup could break the SU(2) invariance of the hopping rates for spin-1 atoms in spin-independent lattices, and how the simulation of systems subjected to three-body repulsion could benefit from it [41]. Here, we extend this idea further and show that the same setup allows for the realization of hopping operators that modify the atomic hyperfine state. Combining this trapping scheme with Fermi gases, we show that this platform would open a new route towards the simulation of high-energy physics and topological insulators.

This paper is organized as follows. In section 2, we describe qualitatively the idea of using an optical superlattice to realize a general hopping operator for a multi-species cold gas of alkalis. Further analysis and technical details are given in section 3, where we also present some numerical results that support the possibility of controlling spin-flipping tunneling in this platform. The reader not interested in these technical details may skip this content without prejudicing the comprehension of the following sections. Some final remarks on the proposal are presented in section 4. In section 5, we discuss possible applications of the described scheme, focusing on relativistic theories and topological insulators, and trying to give a list of the most interesting phenomena that could be explored. Finally, we present our conclusions in section 6.

2. The setup and the idea

We consider the following atomic 3D optical potential:

$$V(\mathbf{x}) = -V_0 \sum_{j \in \{1,2,3\}} [\cos^2(qx_j) + \xi \cos^2(2qx_j)], \quad (1)$$

⁸ The Kavli Institute for Theoretical Physics program ‘Beyond Standard Optical Lattices’ (<http://www.kitp.ucsb.edu/activities/dbdetails?acro=boptilatt10>).

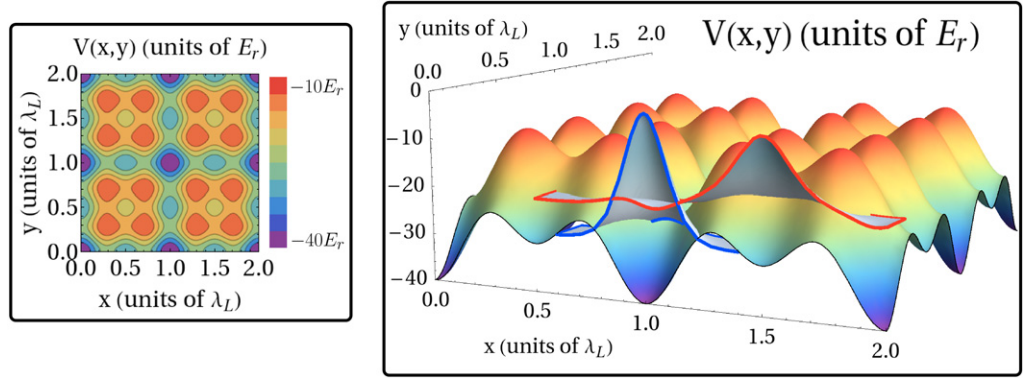


Figure 1. Optical superlattice potential of equation (1) in the 2D case, with parameters $V_0 = 10E_r$ and $\xi = 1$. Left: the potential is characterized by a square geometry of main minima; in the middle of each link an intermediate minimum is also present. Right: if the lattice is deep enough, the spectrum of the system features two energy bands whose Wannier functions are localized in the main minima and in the secondary minima, as plotted in the figure.

where $\mathbf{x} = (x_1, x_2, x_3)$, $q = 2\pi/\lambda_L$ (λ_L is the wavelength of the laser), and where $V_0, \xi > 0$ represent the potential amplitudes. The low-energy structure of this potential is a cubic array of the main minima separated by ‘secondary’ minima located in the middle of each lattice link (see figure 1). We note that additional higher-order minima are also present, but will not play any role in the phenomena discussed in this paper. Due to the specific form of the potential in equation (1), the Hamiltonian can be divided into three independent terms, each one depending on one of the three couples of conjugate operators, $\{x_i, p_i\}_{i \in 1,2,3}$. Consequently, the Bloch functions of the n th band with energy $E_n(\mathbf{p})$ can be written as $\psi_{n,\mathbf{p}}(\mathbf{x}) = \prod_j \psi_{n,p_j}(x_j)$. In order to discuss the effects occurring on the scale of one lattice site, Wannier functions can be introduced for each band

$$w_{n,\mathbf{R}}(\mathbf{x}) = \frac{1}{V} \int e^{-i\mathbf{R}\cdot\mathbf{p}} \psi_{n,\mathbf{p}}(\mathbf{x}) d\mathbf{p} = w_{n,R_1}(x_1) w_{n,R_2}(x_2) w_{n,R_3}(x_3).$$

Like Bloch functions, Wannier functions belonging to different bands form an orthonormal basis, and one can thus expand the Hamiltonian in such a basis. Since the Wannier functions are not eigenstates of the Hamiltonian, this expansion leads to a Hubbard model describing the tunneling of atoms between neighboring sites, together with a local on-site interaction coming from the scattering of the cold gas [42].

This setup can be used for the simulation of a lattice field theory, where the field operators are identified with the atomic creation–annihilation operators in the Wannier basis of the lowest-energy band (i.e. the states localized in the main minima of the lattice). Conversely, higher-energy bands provide auxiliary levels that shall be used as a resource to tailor the tunneling processes. The main result of this paper is the claim that a complicated though not unfeasible combination of current technologies leads us to the realization of the following Hamiltonian:

$$H_{\text{sys}} = \sum_{\mathbf{r}\mathbf{v}} \sum_{\tau\tau'} t_{\mathbf{v}} c_{\mathbf{r}+\mathbf{v}\tau}^\dagger [U_{\mathbf{v}}]_{\tau'\tau} c_{\mathbf{r}\tau} + \sum_{\mathbf{r}} \sum_{\tau\tau'} \Omega c_{\mathbf{r}\tau'}^\dagger [\Lambda]_{\tau'\tau} c_{\mathbf{r}\tau} + \text{h.c.} \quad (2)$$

Here, we are considering a multi-species fermionic scenario with many hyperfine levels of the same atom: $c_{\mathbf{r}\tau}^\dagger$ ($c_{\mathbf{r}\tau}$) creates (annihilates) a fermion with hyperfine spin τ localized in the

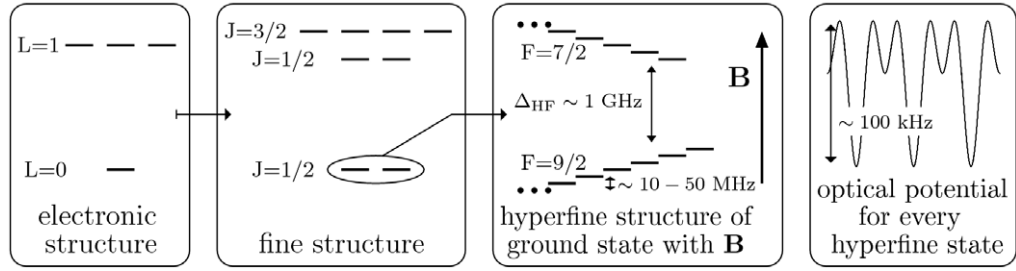


Figure 2. Sketch of the atomic structure of ^{40}K : from the electronic structure (\mathbf{L} is the electronic angular momentum) to the fine structure ($\mathbf{J} = \mathbf{L} + \mathbf{S}$, where \mathbf{S} is the electronic spin) to the hyperfine structure ($\mathbf{F} = \mathbf{J} + \mathbf{I}$, where \mathbf{I} is the nuclear spin). The latter is drawn in the specific case of an external magnetic field present. The last box shows the optical spin-independent potential which traps equally all the hyperfine levels.

main minima of the superlattice at $\mathbf{r} = m_1 \mathbf{a}_1 + m_2 \mathbf{a}_2 + m_3 \mathbf{a}_3$, where $m_j \in \{1 \cdots L_j\}$, L_j stands for the number of lattice sites along the x_j -axis, and \mathbf{a}_j is the lattice spacing in the j th direction. The parameter $t_{\hat{\nu}}$ stands for the strength of the laser-assisted tunneling in the $\hat{\nu}$ direction, with $\hat{\nu} \in \{\mathbf{a}_1, \mathbf{a}_2, \mathbf{a}_3\}$, which shall be described below. The operators $U_{\hat{\nu}}$ describe the tunneling from \mathbf{r} to $\mathbf{r} + \hat{\nu}$ and are a common feature of lattice gauge theories. We have included an on-site Raman term Λ , of strength Ω , that induces a certain transition between the hyperfine states. Note that we use Gaussian units and $\hbar = 1$. We describe some interesting applications of a quantum simulator based on the Hamiltonian (2) in section 5. In particular, we focus on the relevant phenomena for non-interacting theories, which can be realized either with dilute systems or by employing Feshbach resonances (see, e.g., [6, 7]).

Let us note that the control of homogeneous tunneling for a single-species atomic gas is straightforward, and would not even require the superlattice ($\xi = 0$) [43]. Moving to a many-species case, one runs into the problem that a general hopping operator also entails terms flipping the atomic hyperfine spin (simply referred to as *spin* in the following), which are not easily engineered. Here, we propose to realize such couplings by combining Raman transfers and a bi-chromatic superlattice ($\xi \neq 0$ in equation (1)). The proposal can be applied to all the alkalis notwithstanding their bosonic or fermionic nature. In the following, however, we shall focus on the fermionic scenario, which is best explained with the following practical example.

Let us consider an ultra-cold cloud of non-interacting ^{40}K atoms in the presence of a magnetic field of intensity B . Such a field lifts the spin degeneracy within the two atomic hyperfine manifolds of the ground state, $F = 9/2$ and $F = 7/2$, according to the following relations (see also figure 2):

$$E_{9/2, m_F} = +g_F \mu_B B m_F, \quad E_{7/2, m_F} = \Delta_{\text{HF}} - g_F \mu_B B m_F, \quad (3)$$

where m_F is the projection of the hyperfine spin along the quantization axis defined by the magnetic field, μ_B is the Bohr magneton, g_F is the hyperfine Landé factor and Δ_{HF} stands for the hyperfine splitting. These hyperfine levels are all trapped into the same spin-independent optical potential (1). Depending on the lattice theory we want to simulate, we select a subset of these hyperfine levels described theoretically by creation–annihilation operators in the lattice sites. We then identify such fields with the components of the lattice field theory to be simulated. This

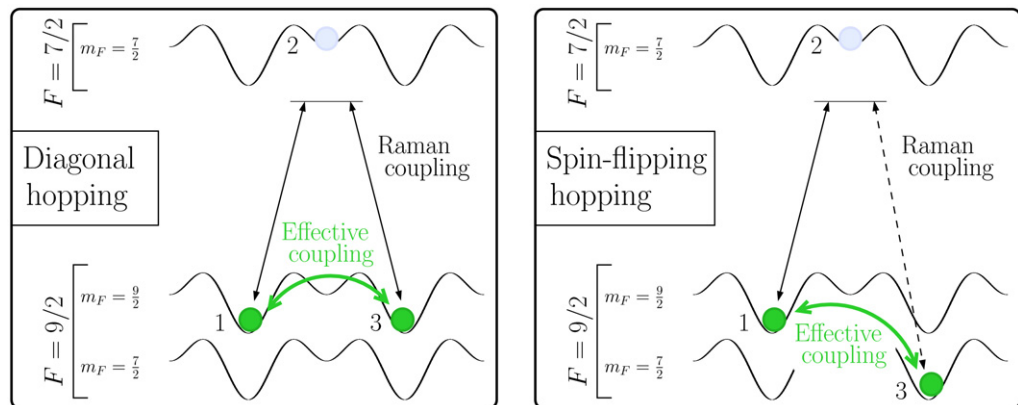


Figure 3. Sketch of laser-assisted tunneling induced in the presence of a superlattice. Two physical hyperfine states belonging to the $F = 9/2$ manifold are connected via Raman couplings with the intermediate level of an auxiliary state belonging to the $F = 7/2$ manifold. If the coupling is detuned enough, the $F = 7/2$ level can be adiabatically eliminated: no population is left there and an effective coupling is engineered between neighboring sites. Left: scheme for a spin-preserving (i.e. diagonal) hopping. Right: scheme for a spin-flipping hopping.

leads us to divide the hyperfine levels into two subsets: the subset of ‘physically meaningful’ states, which belong to the hyperfine manifold $F = 9/2$, and the usually larger subset of auxiliary levels that shall be used to assist the tunneling and create the desired hopping operator.

Regarding the hopping operator in equation (2), we address each of its matrix elements $[U_v]_{\tau'\tau}$ separately. Given a matrix element (i.e. once we have identified the initial and final hyperfine levels to be connected by the assisted tunneling), we choose an auxiliary level belonging to the hyperfine manifold $F = 7/2$ trapped in the middle of the link. These levels provide intermediate ‘bus’ states that shall be used as a resource to assist the tunneling as follows. The couplings between the atoms in the main sites, \mathbf{R}_1 , and the ‘bus’ states, \mathbf{R}_2 , are realized via optical two-photon Raman processes transferring a net momentum \mathbf{q}_r . They have a mathematical expression proportional to the overlap integral of the initial and final Wannier functions: $\int w_{n_2, \mathbf{R}_2}^*(\mathbf{x}) e^{i\mathbf{q}_r \cdot \mathbf{x}} w_{n_1, \mathbf{R}_1}(\mathbf{x}) d\mathbf{x}$. This integral is not zero because of the term $e^{i\mathbf{q}_r \cdot \mathbf{x}}$, which is of course relevant only if $2\pi/|\mathbf{q}_r|$ is of the order of the lattice spacing. Since this regime cannot be achieved with microwave transitions, one is motivated to employ two-photon Raman transitions. Interestingly enough, it is possible to eliminate adiabatically the intermediate level and obtain an effective four-photon coupling between neighboring sites (see figure 3). We stress that different matrix elements can be engineered at the same time thanks to the magnetic-field splitting of the hyperfine levels (3): the involved atomic transitions become non-degenerate and can be individually addressed with different Raman couplings. Furthermore, the use of coherent laser light for the Raman transitions entails the additional advantage of being able to deal with complex phases and thus to realize complex gauge structures at will. The realization of the non-diagonal matrix elements requires the lattice to be slightly staggered, a technique discussed also in [16]. The on-site term Λ in equation (2) can be performed with standard technology based on microwave transitions, or Raman transitions carrying negligible momentum. Furthermore, these

Table 1. Numerical values of a possible 3D optical bi-chromatic superlattice (1) for ^{40}K used in section 3 for numerical simulations. We characterize the properties of the two energy bands, which exhibit Wannier functions localized, respectively, in the main and secondary minima, by listing the energy expectation value $\langle E_i \rangle$ of the most localized Wannier function and the bandwidth ΔE_i . Finally, we argue that atoms trapped in optical lattices show a hierarchy of typical energies which can be actively exploited to engineer non-trivial hopping operators.

λ_L	$\sim 738 \text{ nm}$	$E_r = \frac{\hbar^2}{2m\lambda_L^2}$	9.17 kHz
V_0	$10E_r$	ξ	1
$\langle E_1 \rangle$	$-13.909 \times 3E_r$	$\langle E_2 \rangle$	$(-13.909 \times 2) - 6.364E_r$
ΔE_1	$0.024E_r$	ΔE_2	$0.995E_r$
ΔE_1	216.7 Hz	ΔE_2	9120.1 Hz
Δ_{HF}	1.286 GHz	$g_F \mu_B$	$0.22 \times 1.34 \text{ MHz G}^{-1}$
$\langle E_2 - E_1 \rangle$	69.160 kHz	Staggering	10 kHz

terms can also be exploited to correct spurious on-site couplings which may be induced by the laser scheme. Summarizing, this proposal tries to exploit a hierarchy of energies characterizing atomic gases in optical lattices in order to assist the tunneling between neighboring sites with controlled adiabatic eliminations (see table 1).

We stress here that the proposal does not exploit any selection rule on the polarization properties of the light, but rather relies only on energy-based selection rules, i.e. on the detuned atomic transitions induced by the magnetic field. Even though in low-dimensional setups the specific experimental implementation could benefit from polarization selection rules, they are not necessary and there is no fundamental limitation to the extension of the setup to more dimensions.

3. Realization of spin-dependent hopping operators

In this technical section, we theoretically and numerically confirm the qualitative scheme presented above. We study two simple but important cases: the realization of diagonal and non-diagonal hopping operators for a two-species atomic gas. These can be considered as the main building blocks needed to realize any tunneling operator even in situations with more than two atomic species. In order to make this paper self-contained, we reproduce in this section some of the results presented in [41]. The discussion there was limited to the realization of a Raman-assisted diagonal tunneling. In this work, we extend it to a regime where one can control a non-diagonal hopping, which turns out to be the key ingredient for the versatility of our quantum simulator.

3.1. Coupling between different hyperfine manifolds

The most fundamental ingredient of this proposal is the possibility of using Raman processes to induce controlled atomic transitions between different hyperfine states of the electronic ground state $L = 0$ (L is the total electronic angular momentum). These transitions are realized with two lasers via adiabatic elimination of the electronically excited manifold $L = 1$. In the following,

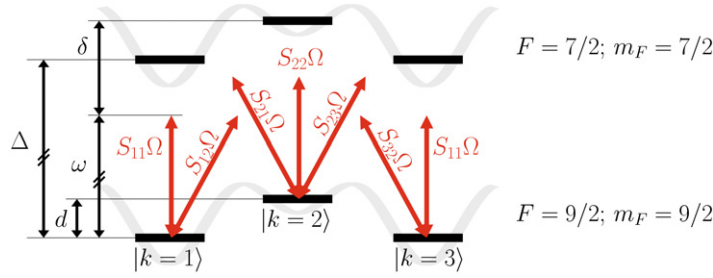


Figure 4. The ‘6-level model’ used to model the spin-preserving (diagonal) hopping of $F = 9/2$, $m_F = 9/2$. The auxiliary state $F = 7/2$, $m_F = 7/2$ has been chosen. The center-of-mass quantum number is k . Energies are not to scale; the orders of magnitude of the parameters are the following: $d \sim 10\text{--}100$ kHz, $\delta \sim 100\text{--}300$ kHz and $\Delta \sim 1\text{--}10$ GHz. We propose to adiabatically eliminate the upper manifold and to study the dynamics of the lowest one with an effective Hamiltonian H_{pert} (8).

we address the atomic levels as $|L, \alpha, k\rangle$, with α labeling the hyperfine degrees of freedom (see also figure 2 for some insights into the internal structure of ^{40}K), and k the quantum numbers of the center-of-mass wavefunction (in our case, the Wannier functions of the optical potential). As discussed in [41], the induced Raman coupling between the states $|0, \alpha, k\rangle$ and $|0, \alpha', k'\rangle$ can be written as follows:

$$\tilde{\Omega}_{\alpha'k';\alpha k}(t) = S_{k'k} \Omega_{\alpha'\alpha} e^{-i\omega t}. \quad (4)$$

This expression clearly factorizes the following contributions:

- the time dependence of the effective coupling and its effective frequency, which is the difference between the frequencies of the two lasers $\omega = \omega_1 - \omega_2$;
- the dependence on the center-of-mass degrees of freedom, $S_{k'k} = \langle k' | e^{-i(\mathbf{p}_2 - \mathbf{p}_1) \cdot \mathbf{x}} | k \rangle$, where \mathbf{p}_1 and \mathbf{p}_2 are the momenta of the two lasers;
- the dependence on the initial and final internal states and on the polarization properties of light, $\Omega_{\alpha'\alpha}$, which is a function of the dipole matrix elements between the initial (final) state and the excited levels.

Next, we specify (4) to the superlattice setup of section 2, i.e. we will consider Raman transitions in the presence of lattices characterized by a Wannier function trapped in the middle of each link.

3.2. Developing an effective ‘6-level model’

Let us address the simulation of a theory characterized by two-component fields. Following the discussion of section 2, we take two states of the $F = 9/2$ manifold of ^{40}K , for instance $|9/2; m_F = 7/2\rangle$ and $|9/2; m_F = 9/2\rangle$, and map them into the theory to be simulated. Here and in the following subsections, we discuss the laser-assisted hopping in the diagonal case (m_F preserved while hopping) and the non-diagonal case (m_F flipped while hopping).

For the diagonal case, we develop the ‘6-level model’ depicted in figure 4. We consider one physically meaningful state, say $|F = 9/2, m_F = 9/2\rangle$, and one auxiliary state, say $|F = 7/2, m_F = 7/2\rangle$. Moreover, we consider different Wannier states for each of them, two localized

in main sites ($k = 1$ and 3) and one in the intermediate link ($k = 2$). The model includes the effects of undesired couplings and additional levels, and its limitations, together with the approximations on which it relies, will be discussed at the end of the paragraph. We can identify the states with the short notation $|F, k\rangle$ rather than with the longer previous one $|0\alpha k\rangle$. Below, we give an analytical estimate of the population transfer rate, whereas in the next subsections we present the numerical time evolution for physically interesting cases.

The model is parameterized by six relevant couplings between the different Wannier functions $S_{k'k}$ (see figure 4) whose properties are listed below. We exploit the existence of theorems which guarantee the possibility, in our case, of considering three real and exponentially localized Wannier functions $w_j(\mathbf{x})$, $j \in \{1, 2, 3\}$ [44]. We write the parameters $S_{k'k}$ factorizing out the space dependence of the coupling $e^{i\mathbf{q}_t \cdot \mathbf{x}_j}$, where \mathbf{x}_j is the position of the point around which the Wannier function $w_j(\mathbf{x})$ is localized,

$$S_{k'k} = e^{i\mathbf{q}_t \cdot \mathbf{x}_k} \int w_{k'}^*(\mathbf{x} - \mathbf{x}_{k'} + \mathbf{x}_k) e^{i\mathbf{q}_t \cdot \mathbf{x}} w_k(\mathbf{x}) d\mathbf{x}, \quad (5)$$

$$S_{1,1} = S_{3,3} \neq S_{2,2}, \quad S_{1,3}, S_{3,1} \sim 0. \quad (6)$$

The parameters $S_{1,1}$ and $S_{2,2}$ describe two on-site couplings, whereas $S_{1,2}$ is the coupling between a main site and an intermediately trapped state (see figure 4). The last relation states that couplings between neighboring main sites are negligible. The relation between the other four overlap factors depends on the particular experimental situation. In this case, we are interested in the simplest scenario where a single Raman transition induces all these couplings, which leads us to

$$S_{1,2} = S_{2,1} = e^{2i\mathbf{q}_t \cdot \mathbf{x}_1} e^{i\mathbf{q}_t \cdot (\mathbf{x}_3 - \mathbf{x}_1)} S_{3,2}^* = e^{2i\mathbf{q}_t \cdot \mathbf{x}_1} e^{i\mathbf{q}_t \cdot (\mathbf{x}_3 - \mathbf{x}_1)} S_{2,3}^*.$$

In order to make this scheme simpler, we assume that $\mathbf{q}_t = 2\mathbf{q}_L$ and thus $e^{i\mathbf{q}_t \cdot (\mathbf{x}_2 - \mathbf{x}_1)} = 1$. As we will argue below, transferring a momentum that does not fulfill this requirement is not a problem since the resulting phase can be gauged away. The phase $2\mathbf{q}_t \cdot \mathbf{x}_1$ can also be put to zero for the moment, since its role only becomes important when one needs to give a phase to different matrix elements. In the following, we will also consider situations where the coupling between the lattice sites 2 and 3 could be induced by lasers propagating in the opposite direction, where $S_{1,2} = S_{2,1} = S_{3,2} = S_{2,3}$. Taking these considerations into account, the Hamiltonian reads as follows (see figure 4 for the definitions of δ , Δ and ω):

$$\begin{aligned} H = & d |9/2, 2\rangle\langle 9/2, 2| + (\Delta + d) |7/2, 2\rangle\langle 7/2, 2| + \Delta (|7/2, 1\rangle\langle 7/2, 1| + |7/2, 3\rangle\langle 7/2, 3|) \\ & + \Omega e^{-i\omega t} [S_{1,2} (|7/2, 2\rangle\langle 9/2, 1| + |7/2, 1\rangle\langle 9/2, 2|) \\ & + S_{1,2}^* (|7/2, 2\rangle\langle 9/2, 3| + |7/2, 3\rangle\langle 9/2, 2|) \\ & + S_{1,1} (|7/2, 1\rangle\langle 9/2, 1| + |7/2, 3\rangle\langle 9/2, 3|) \\ & + S_{2,2} |7/2, 2\rangle\langle 9/2, 2|] + \text{h.c.} \end{aligned} \quad (7)$$

Once we apply the unitary transformation

$$\Gamma(t) = \exp[i d (|9/2, 2\rangle\langle 9/2, 2| + |7/2, 2\rangle\langle 7/2, 2|) t],$$

the three levels $|9/2, k\rangle$ become degenerate. In the case the three inequalities $|S_{i,j}\Omega|/(\delta - d) \ll 1$ are fulfilled, it is possible to use second-order perturbation theory in

order to develop an effective Hamiltonian describing the dynamics within the sub-manifold we are interested in, namely

$$\begin{aligned}
H_{\text{pert}}/\Omega^2 = & - \left(\frac{|S_{1,1}|^2}{\delta-d} + \frac{|S_{1,2}|^2}{\delta} \right) [|9/2, 1\rangle\langle 9/2, 1| + |9/2, 3\rangle\langle 9/2, 3|] \\
& - \left(\frac{|S_{2,2}|^2}{\delta-d} + 2\frac{|S_{1,2}|^2}{\delta-2d} \right) |9/2, 2\rangle\langle 9/2, 2| - \frac{S_{1,2}^2}{\delta} |9/2, 3\rangle\langle 9/2, 1| + \text{h.c.} \\
& - \left[\frac{S_{1,2}^* S_{1,1}}{2} \left(\frac{1}{\delta-d} + \frac{1}{\delta-2d} \right) e^{idr} + \frac{S_{2,2}^* S_{1,2}}{2} \left(\frac{1}{\delta-d} + \frac{1}{\delta} \right) e^{idr} \right] \\
& \times [|9/2, 2\rangle\langle 9/2, 1| + |9/2, 2\rangle\langle 9/2, 3|] + \text{h.c.}
\end{aligned} \tag{8}$$

Remarkably enough, this Hamiltonian leads to the desired transfer rate of population from level $|9/2, 1\rangle$ to $|9/2, 3\rangle$, and vice versa. The main contribution is the direct coupling

$$-J_{13}^{(1)} e^{i2\phi} = -\frac{|S_{1,2}|^2 \Omega^2}{\delta} e^{i2\phi}, \quad \phi = \arg S_{1,2}. \tag{9}$$

A second contribution, which in our system will prove to be non-negligible, comes from a sort of ‘adiabatic elimination’ of the level $|9/2, 2\rangle$, namely

$$-J_{13}^{(2)} = -\frac{\langle 9/2, 3|H_{\text{pert}}|9/2, 2\rangle \langle 9/2, 2|H_{\text{pert}}|9/2, 1\rangle}{\langle 9/2, 2|H_{\text{pert}}|9/2, 2\rangle - \langle 9/2, 1|H_{\text{pert}}|9/2, 1\rangle + d}. \tag{10}$$

Accordingly, we have derived the desired effective Hamiltonian where the Raman lasers assist the hopping of the physically meaningful $F = 9/2$ levels, after the auxiliary $F = 7/2$ bus states have been adiabatically eliminated. In the following sections, we shall address the range of validity of the approximations leading to this Hamiltonian, and compare it with the exact numerical investigation of the initial Hamiltonian (7).

We want to stress here that even if the integrals in the definition (5) of the $S_{kk'}$ can be complex numbers, this does not have any physical influence on this proposal. Indeed, even if the effective coupling between neighboring main sites $-J$ was complex, its spatially uniform phase can be gauged away with a space-dependent unitary transformation (even in the case of periodic boundary conditions). Conversely, the non-uniform phase coming from the $e^{i\mathbf{q}_t \cdot \mathbf{x}_k}$ factor, which arises when \mathbf{q}_t is not parallel to the direction of the hopping it assists, cannot be gauged away even in the presence of open boundary conditions. Such a phase, which is not related to the fact that the integrals in (5) are complex, can be used to simulate an external uniform magnetic field [15, 16]. Finally, we stress that in our setup, where the tunneling along each axis is induced by lasers propagating parallel to the axis itself, both complex phases can be gauged away. In order to simulate a magnetic field, therefore, one should move slightly away from this configuration and engineer a Raman coupling whose effective transmitted momentum does not run parallel to the links of the lattice. We will not consider this situation in this paper because the models of interest in section 5 do not require such a space-dependent phase.

3.3. Range of validity of the ‘6-level model’

The presented ‘6-level model’ strongly relies on two approximations:

- (i) considering the bands of the lattice as being flat,
- (ii) neglecting delocalized higher-energy free states.

If these approximations are not justified for a given experimental configuration, spurious population transfers to next-neighboring sites would arise.

The approximation (i) is required to fulfill the core idea of the proposal, namely the adiabatic elimination of the intermediate level. This is demonstrated with a model which considers only a subset of the Hilbert space spanned by the real eigenstates of the Hamiltonian (Bloch functions), considering just three of their linear combinations (the Wannier functions $w_{k=1}(\mathbf{x})$, $w_2(\mathbf{x})$ and $w_3(\mathbf{x})$). This is equivalent to approximating the dispersion laws of the band as flat, neglecting thus possible curvature effects, and is legitimized as long as the width of the band is much smaller than the detuning of the transition $\delta - d$. In the case that the degeneracy of the Bloch functions cannot be assumed, all the Bloch functions should be considered in order to quantitatively estimate the spurious effects cited above. In general, this issue sets a trade-off for the relative depth ξ of the secondary lattice in (1): on the one hand, a shallow lattice ($\xi < 1$) is desirable because the Wannier function of the intermediate minimum $w_{k=2}(\mathbf{x})$ is not strongly localized and laser-induced transitions are favored ($|S_{1,2}| \sim |S_{1,1}|$). On the other, the more the wavefunction is delocalized, the more the band bends, eventually becoming parabolic at $\mathbf{k} = 0$ with a bandwidth comparable to the detuning. In our numerical simulations we consider $\xi = 1$, which is a reasonable compromise.

Regarding the issue (ii), higher-energy bands could become important in the presence of intense Raman transitions Ω and large detunings $\delta - d$, which couple them to the lowest-band states. The presented analytical and numerical studies do not take into account these effects since they consider only three Wannier functions and effectively only two bands, even though including bands with localized Wannier functions would just imply a renormalization of the numerical coefficients $S_{k,k'}$. A different problem is the case of high-energy strongly parabolic bands whose Wannier functions are not strongly localized. The effect of such states is not considered by our model, which is that of spreading population among many next- and further-neighboring main sites. From an experimental point of view, we expect a trade-off to arise between a large detuning regime, allowing powerful lasers and strong effective couplings with noisy spurious population transfers, and a small detuning one, with clean but small couplings.

3.4. Diagonal hopping operator

We now explicitly study the possibility of realizing a diagonal tunneling operator. We numerically simulate the Hamiltonian (7) with a simple Runge–Kutta algorithm. We did not include in the simulation hyperfine states different from $|F = 9/2, m_F = 9/2\rangle$ and $|F = 7/2, m_F = 7/2\rangle$ because they are strongly detuned from those we are considering. However, for completeness, we include the presence of a second Raman coupling, which would be needed to induce the hopping of $|F = 9/2; m_F = 7/2\rangle$, and check that it is unimportant.

We show in figure 5 the numerical results. The realistic parameters used in this simulation are listed in table 2. The population is coherently transferred between two neighboring levels and only a negligible fraction is lost in auxiliary states. Regarding the validity of the ‘6-level model’, for the lattice considered here, the bandwidths of the two bands are 0.2 and 9.1 kHz, respectively, which should be compared with the considered detuning of 300 kHz. In these and the following simulations, the employed numerical values have only illustrative purpose and other regimes could be considered.

To estimate the accuracy of the assisted hopping operator, we compute the fidelity of generating a particular target spin state at site $k = 3$ in the internal state $\{F_t, m_{F,t}\}$,

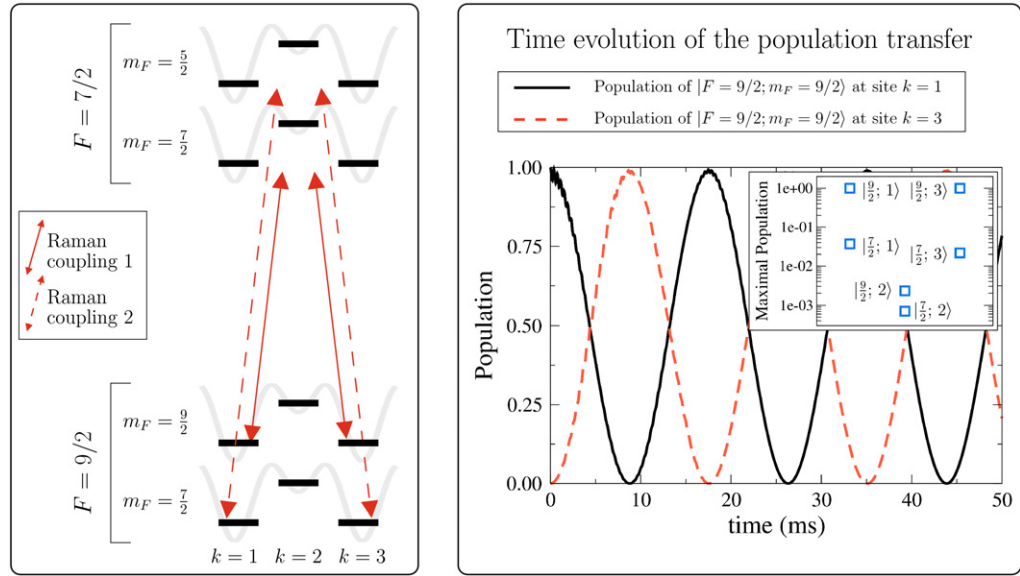


Figure 5. Left: sketch of the scheme proposed for the realization of a diagonal hopping operator (energies are not to scale). Raman coupling 1 (2) connects the $|F = 9/2, m_F = 9/2\rangle$ ($|F = 9/2, m_F = 7/2\rangle$) state to its auxiliary state. Detuning allows independent control of the hopping rates. Right: exact time evolution of the ‘6-level model’ (7), showing the coherent population transfer between sites 1 and 3 of the spin state $|F = 9/2, m_F = 9/2\rangle$. The parameters used are listed in table 2. The inset shows the maximal populations of the six considered levels labeled $|F, k\rangle$ as in (7) and shows that only a small fraction of the population is lost in auxiliary levels.

i.e. $|\psi_t\rangle = |3, F_t, m_{F,t}\rangle$, for an atom that is initially populating the site $k = 1$ in the internal state $\{F_i, m_{F,i}\}$, i.e. $|\psi_i\rangle |1, F_i, m_{F,i}\rangle$. Such fidelity can be quantified defining

$$\mathcal{F}^2 = \max_{\tau} |\langle \psi_t | \psi(\tau) \rangle|^2, \quad (11)$$

with $|\psi(\tau)\rangle$ being the time evolved state, which is the amplitude of the oscillations between the sites between which the hopping operator acts. For the presented simulation the fidelity of the stimulated hopping process is $\mathcal{F}^2 > 97\%$. Therefore, these results confirm the plausibility of our scheme to induce laser-assisted tunneling between the atoms sitting in the main minima of the optical lattice. To make the simulation toolbox richer, we now address the possibility of controlling a spin-dependent hopping process.

3.5. Non-diagonal hopping operator

In order to study the realization of the non-diagonal hopping operator, we consider an enlarged 12-level model, which is a generalization of the previous one taking into account more hyperfine states. We want now to transfer population between the manifolds $|F = 9/2, m_F = 9/2\rangle$ and $|F = 9/2, m_F = 7/2\rangle$ and consider as auxiliary states $|F = 7/2, m_F = 7/2\rangle$ and $|F = 7/2, m_F = 5/2\rangle$.

Table 2. Parameters used for the numerical simulation of the diagonal hopping in subsection 3.4. We list the numerical values of all the main parameters characterizing the atomic transitions and the Raman couplings. The first Raman coupling induces the hopping of $F = 9/2$, $m_F = 9/2$, whereas the second one addresses $F = 9/2$, $m_F = 7/2$ (such states were, however, not considered in the simulation).

Level: $ F, m_F, k\rangle$	Energy	Parameters	
$ 9/2; 9/2; 1\rangle$	$g_F \mu_B B m_F$	Δ_{HF}	1.285 GHz
$ 9/2; 9/2; 2\rangle$	$g_F \mu_B B m_F + d$	$\mu_F B$	40 MHz
$ 9/2; 9/2; 3\rangle$	$g_F \mu_B B m_F$	d	69.160 kHz
$ 7/2; 7/2; 1\rangle$	$\Delta_{\text{HF}} - g_F \mu_B B m_F$	$S_{1,1}$	0.46
$ 7/2; 7/2; 2\rangle$	$\Delta_{\text{HF}} - g_F \mu_B B m_F + d$	$S_{1,2}$	$0.07 + i0.13$
$ 7/2; 7/2; 3\rangle$	$\Delta_{\text{HF}} - g_F \mu_B B m_F$	$S_{2,2}$	0.16

Raman coupling	Ω	ω
1	49.5 kHz	$E_{ 7/2; 7/2; 2\rangle} - E_{ 9/2; 9/2; 1\rangle} - 300$ kHz
2	49.5 kHz	$E_{ 7/2; 5/2; 2\rangle} - E_{ 9/2; 7/2; 2\rangle} - 300$ kHz

$J_{13}^{(1)}$	$J_{13}^{(2)}$	Estimated T	Numerical T
176 Hz	17 Hz	0.018 s	0.017 s

A big issue that must be solved to engineer such a hopping is the appearance of undesired spin-flipping terms induced by the laser (see figure 6). In this paper, we consider the possibility of staggering the lattice with an additional optical field in order to lift the degeneracy between the different sites of the optical lattice, in the same manner as [16]. Such staggering can be done also in three dimensions since the cubic lattice is bipartite, and we consider staggering values of 10–15 kHz.

Figure 7 sketches the experimental scheme we have in mind and shows the exact time evolution of the population transfer between the two levels of $F = 9/2$ in two neighboring sites. Interestingly enough, we show a flip of the Zeeman spin during the tunneling process and thus obtain the promised spin-dependent hopping operator. The parameters of the simulation can be found in table 3. The fidelity of the simulated hopping process is $\mathcal{F}^2 > 88\%$. A meaningful estimate is made difficult here by the fast oscillations appearing on top of the slow Rabi oscillations; we give here a lower bound, given by the lower envelope of the curve.

In comparison with figure 5, the Rabi oscillations of figure 7 present additional fast oscillations of small amplitude and also do not reach perfect state transfer. The reason can be found in the inset of figure 7, which shows that a fraction of the population has been transferred to the states $|F = 9/2; m_F = 7/2; 1\rangle$ and $|F = 9/2; 9/2; 3\rangle$. This is the result of the on-site spin-flipping transitions, which have to be avoided using the lattice staggering. The fact that they are not completely suppressed means that the simulation uses parameters which are not optimal; in particular, the system would benefit from larger staggering values. Finally, we also mention

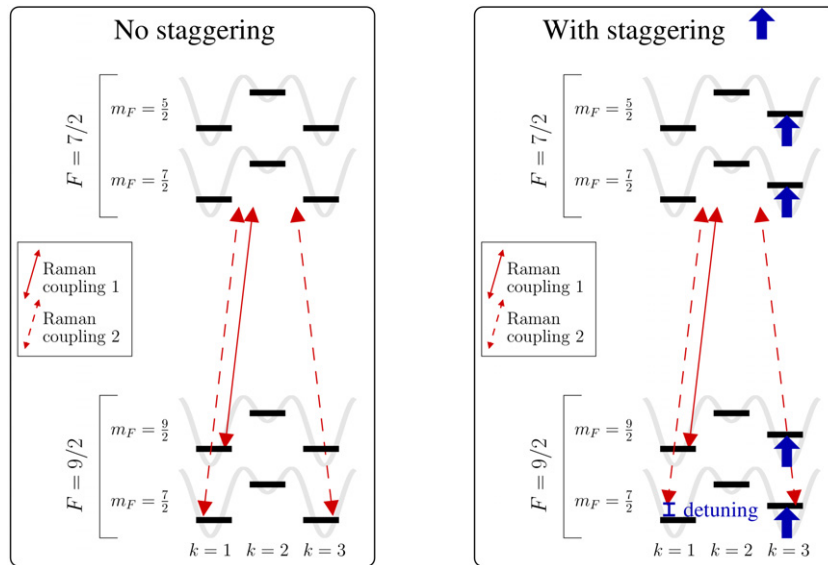


Figure 6. Left: the realization of a spin-flipping hopping operator suffers from the problem that undesired on-site spin-flipping processes could spontaneously arise. Right: the solution to this problem comes from the introduction of a staggered lattice. The on-site spin-flipping process is detuned from the atomic transition and its contribution is negligible with respect to the hopping process, which is resonant with the atomic transition.

that the lattice staggering introduces an asymmetry between the two sites. As a consequence, the different ac-Stark shifts of the levels with $k = 1$ and $k = 3$ due to the Raman beams must be taken into account when selecting the laser frequencies. We note that these corrections turn out to be crucial for achieving an optimal population transfer.

We have demonstrated that the Raman-assisted tunneling scheme leads to both diagonal and non-diagonal tunneling events. Note that the achieved fidelities above $\mathcal{F}^2 > 88\%$ highlight the accuracy of our scheme, and show that only energy-based selection rules, together with lattice staggering, suffice to allow the desired tunneling.

4. From a spin-dependent hopping operator to a quantum simulator

In the previous section, we discussed how the superlattice geometry could be used to create non-trivial hopping operators on each link. Here we want to assemble these ingredients and discuss how to use them to engineer a quantum simulator in arbitrary dimensions, considering the advantages and disadvantages of the proposal.

First of all, we stress that the lasers needed to engineer the hopping along one direction must transfer momentum along that same direction (see equation (6)). Therefore, just by controlling the beam propagation directions, we can tailor different tunneling operators along each axis. This is an important feature which will be largely exploited in the proposals listed in section 5 (see, e.g., tables 5 and 6, which list the different hopping operators that must be engineered for each particular model of interest). This kind of *directionality selection rule* is also responsible for avoiding the population of higher-order minima which do not lie on

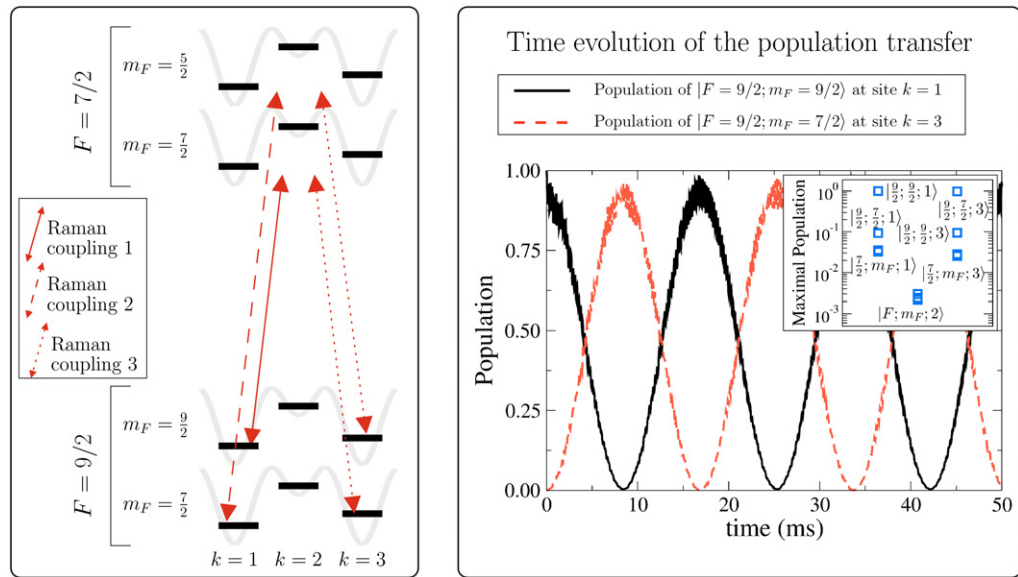


Figure 7. Left: sketch of the scheme proposed for the realization of a non-diagonal hopping operator (energies are not to scale). Raman couplings 1, 2 and 3 connect the $|F = 9/2, m_F = 9/2\rangle$ and $|F = 9/2, m_F = 7/2\rangle$ states to the auxiliary states. Detuning allows independent control of the hopping rates. Right: exact time evolution of the ‘12-level model’ introduced in subsection 3.5 and generalizing (7). We show the coherent population transfer between sites 1 and 3 of the spin state $|F = 9/2, m_F = 9/2\rangle$ and $|F = 9/2, m_F = 7/2\rangle$. The parameters used are listed in table 2. The inset shows the maximal populations of the 12 considered levels labeled $|F, m_F, k\rangle$ and shows that only a fraction of the population is lost in auxiliary levels.

the edges of the unit lattice cell. Since they are not connected to the main minima by a line parallel to a Cartesian axis, we do not consider any momentum transfer along this direction, and thus the formal orthogonality of the Wannier functions localized in those minima is never lifted.

Due to the very general formulation of the superlattice potential, the setup is well suited also to work in two and one dimensions. Moreover, in 1D it is possible to use polarization selection rules to selectively couple different atomic levels. As a short-term goal, it would be very interesting to understand what is the most interesting physics that could be simulated in a 1D system, where the presence of more symmetries could lower the experimental intricacies. We partially address this question in section 5, where we argue that several 1D topological phases can be realized. In the 3D (2D) case, only energy-based selection rules are reliable; the discussion in section 3 already showed that these are enough. Let us stress that if the spin quantization axis \hat{B} , given by the external magnetic field, is not chosen along a highly symmetric axis of the lattice, even a Raman coupling polarized with respect to its propagation axis, i.e. one of the axes of the lattice, can contain all the polarizations in the basis of \hat{B} . As sketched in figure 8, the polarization matching the addressed transition will drive it, whereas the other ones, being detuned, will have negligible effect.

Table 3. Parameters used for the numerical simulation of the non-diagonal hopping in subsection 3.5. We list the numerical values of the main parameters characterizing atomic transitions and Raman couplings. The reported frequencies of the Raman couplings are approximate because some additional tuning is needed to compensate for the different Stark shifts for states with $k = 1$ and $k = 3$ arising due to Raman dressing in the presence of staggering. Perfect matching of the atomic transition becomes difficult and imperfections are responsible for the non-clean population transfer in figure 7. Larger staggering values would help.

Level: $ F, m_F, k\rangle$	Energy	Parameters
$ 9/2; 9/2; 1\rangle, 9/2; 7/2; 1\rangle$	$g_F \mu_B B m_F$	Δ_{HF} 1.285 GHz
$ 9/2; 9/2; 2\rangle, 9/2; 7/2; 2\rangle$	$g_F \mu_B B m_F + d$	$\mu_F B$ 40 MHz
$ 9/2; 9/2; 3\rangle, 9/2; 7/2; 3\rangle$	$g_F \mu_B B m_F + 15 \text{ kHz}$	d 69.160 kHz
$ 7/2; 7/2; 1\rangle, 7/2; 5/2; 1\rangle$	$\Delta_{\text{HF}} - g_F \mu_B B m_F$	$S_{1,1}$ 0.46
$ 7/2; 7/2; 2\rangle, 7/2; 5/2; 1\rangle$	$\Delta_{\text{HF}} - g_F \mu_B B m_F + d$	$S_{1,2}$ $0.07 + i0.13$
$ 7/2; 7/2; 3\rangle, 7/2; 5/2; 1\rangle$	$\Delta_{\text{HF}} - g_F \mu_B B m_F + 15 \text{ kHz}$	$S_{2,2}$ 0.16

Raman coupling	Ω	ω
1	49.5 kHz	$\sim E_{ 7/2;7/2;2\rangle} - E_{ 9/2;9/2;1\rangle} - 300 \text{ kHz}$
2	49.5 kHz	$\sim E_{ 7/2;5/2;2\rangle} - E_{ 9/2;7/2;1\rangle} - 300 \text{ kHz}$
3	49.5 kHz	$\sim E_{ 7/2;7/2;2\rangle} - E_{ 9/2;7/2;3\rangle} - 300 \text{ kHz}$

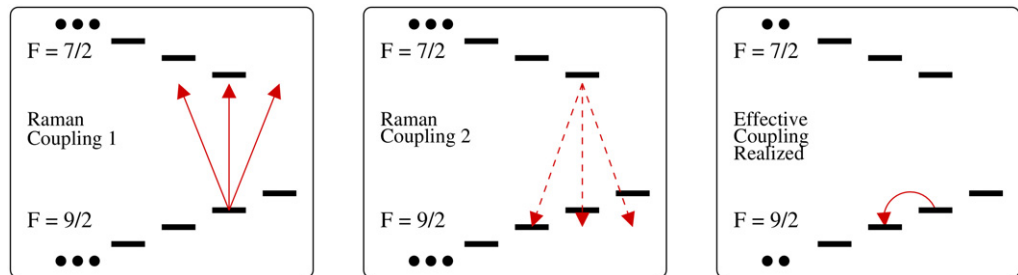


Figure 8. Energy selection rule. The scheme does not rely on any polarization selection rule and therefore does not face any fundamental problem once considered in two and three dimensions. If the Raman coupling is not polarized with respect to the quantization axis of the hyperfine levels, all the polarizations are present, even though with different intensities. The first and second Raman couplings therefore drive an effective population transfer between two states with different hyperfine spins even without engineering polarized couplings; energy detuning is enough.

Unfortunately, energy-based selection rules do not prevent, in the case of spin-flipping operators, spurious on-site spin-flipping couplings. We proposed to solve this issue by staggering the optical lattice, i.e. lifting the degeneracy of the lattice sites of some tens of kHz (see also the discussion in [16]). One should also mention that the diagonal hopping operators

can still be engineered in the presence of such staggering, with the only additional issue of using two Raman couplings (as in the non-diagonal case) to match the energy difference between sites.

Regarding the form of the staggering potential, we propose to use a separable one: $V_{\text{st1}}(\mathbf{x}) = V(\mathbf{x}) - V_2 \sum_i \cos^2\left(\frac{q x_i}{2}\right)$. The separability of the potential V_{st1} allows us to apply the developed theory and in particular the directionality selection rule. The absolute value of the energy differences between neighboring sites is $\sim V_2$, which is what we studied in subsection 3.5. A calculation performed using equation (5) shows that given the propagation direction of the Raman couplings, the effective hopping does not depend on whether the initial site was the staggered one or not. Alternatively, we also considered explicitly the case of a 2D lattice staggered by a non-separable potential: $V_{\text{st2}}(\mathbf{x}) = V(\mathbf{x}) - V_2 \cos^2\left(\frac{q x_1 + q x_2 + q x_3}{2}\right)$, which may be of some experimental relevance. The corresponding 2D and 3D Wannier functions are no longer a product of 1D ones and a Raman coupling can induce hopping in the direction transverse to its propagation. We computed numerically the band structure and Bloch functions of the staggered 2D system for the proposed lattice parameters. The wavefunctions differ from those of the case $V_2 = 0.0$ by less than 1% of the averaged maxima of the wavefunctions. This leads us to the conclusion that they can be nicely approximated by product wavefunctions, to which the directionality selection rule applies. Spurious couplings in the orthogonal directions introduce noise which is negligible with respect to the fidelity of the non-diagonal hopping discussed in section 3.5.

Each of the matrix elements of the hopping operators is realized via an effective four-photon process. This means that the spin of the atom can be flipped at most $|\Delta m_F| = 4$: a careful analysis is needed in case one is interested in simulating a theory with more than four fields, because some hopping matrix elements might be non-engineerable.

Finally, the description given in this proposal is essentially at the single-particle level where no many-body effects have been used. As a consequence, the proposal works for both bosons and fermions, which is a valuable result.

Before concluding, we would like to mention some possible technical issues which should be addressed before running an experiment. Firstly, in the absence of an efficient taming of the atomic interactions, which has been assumed throughout the whole paper, the gas could be collisionally unstable; spin exchange and dipolar relaxation could indeed populate non-physical states or even lead to losses. A quantification of such effects strongly depends on the chosen atomic system and is therefore beyond the scope of this paper. Such an estimate would also identify the regime of controlled interactions in which the quantum simulator would explore interacting relativistic field theories and interacting topological insulators (section 5). We leave this topic for future work.

Secondly, in the previous sections we always assumed the possibility of realizing the needed Raman coupling, this technique being currently under development in cold-atom laboratories. We mention here the lifetime issue that one would face in the presence of transitions that are not sufficiently detuned from the excited states. This issue also requires accurate system-dependent quantification before setting up an experiment and is beyond the scope of this paper.

This concludes the part of the paper devoted to a description of the experimental setup. We believe we have provided relevant results supporting the initial claim that it is indeed possible to realize a system whose low-energy structure is described by Hamiltonian (2).

5. Applications of the quantum simulator

In this section, we would like to discuss the use of the described setup as a quantum simulator. We will address a range of lattice field theories for relativistic fermions [45], and explore exotic phases of matter known as topological insulators [46]. In general, the task of a purpose-based quantum simulator is to realize a system described by an effective Hamiltonian H_{eff} that reproduces faithfully the properties of the model to be simulated. In our case, this model corresponds to relativistic lattice fermions H_{rel} or topological insulators H_{top} . The resource to accomplish such a task is the microscopic control over the superlattice setup, which we have argued previously to be described by the Hamiltonian (2), rewritten here for reading convenience,

$$H_{\text{sys}} = \sum_{\mathbf{r}\nu} \sum_{\tau\tau'} t_{\nu} c_{\mathbf{r}+\nu\tau'}^{\dagger} [U_{\nu}]_{\tau'\tau} c_{\mathbf{r}\tau} + \sum_{\mathbf{r}} \sum_{\tau\tau'} \Omega c_{\mathbf{r}\tau'}^{\dagger} [\Lambda]_{\tau'\tau} c_{\mathbf{r}\tau} + \text{h.c.}$$

The main objective in the following subsections is to control and manipulate

- (i) the optical lattice dimension D ,
- (ii) the tunneling strengths t_{ν} ,
- (iii) the spin-dependent hopping operators U_{ν} ,
- (iv) the on-site Raman transitions Ω, Λ ,

such that the Hamiltonian of equation (2) simulates the desired physics, namely

$$H_{\text{sys}}(\{t_{\nu}, U_{\mathbf{r}\nu}, \Lambda, \Omega\}) \rightarrow H_{\text{eff}} \approx H_{\text{rel}}, H_{\text{top}}.$$

From a condensed-matter perspective, exotic phases are frequently associated with strongly correlated regimes and many-body interactions. There are, however, distinguished exceptions to this paradigm, such as graphene [47] and topological insulators [46], where quadratic fermionic Hamiltonians contain a wealth of non-trivial phenomena. In the case of graphene, a 2D layer of graphite, the low-energy carriers can be described by emerging relativistic fermions without mass. On the other hand, topological insulators are exotic holographic phases with an insulating bulk, and a peculiar boundary that hosts robust conducting modes protected by topology arguments. In both cases, the transport properties of the material differ significantly from the standard solid-state theory. The following subsections are an analytical review of many interesting phenomena which could be simulated with our quantum simulator. The discussion provides for every model the specific values for the parameters of Hamiltonian (2) to be engineered and we hope with this effort to provide a tool for bridging the gap between two different communities, experimental atomic physics and theoretical condensed matter physics.

5.1. The zoo of relativistic lattice fermions

The properties of a relativistic spin-1/2 fermion with mass m are described by the Dirac Hamiltonian [48]

$$H = \int d\mathbf{r} \Psi(\mathbf{r})^{\dagger} H_{\text{DI}} \Psi(\mathbf{r}), \quad H_{\text{DI}} = c\boldsymbol{\alpha} \cdot \mathbf{p} + mc^2\beta, \quad (12)$$

where α_{ν}, β are the so-called Dirac matrices fulfilling a Clifford algebra, $\{\alpha_{\nu}, \alpha_{\mu}\} = 2\delta^{\nu\mu}$, $\{\alpha_{\nu}, \beta\} = 0$, and c stands for the speed of light. Here, $\Psi(\mathbf{r})$ is the N_{D} -component fermionic

Table 4. Quantum simulator of naive Dirac fermions. Each translationally invariant hopping operator U_v is expressed in terms of Pauli matrices $\{\sigma_x, \sigma_y, \sigma_z\}$, and a set of dimensionless fluxes $\{\phi_1, \phi_2, \phi_3\}$. We also list a particular representation of the Dirac matrices α_v, β for different spatial dimensions d , together with the important symmetries of the Hamiltonian that depend on Γ . These hopping operators are to be realized using the recipes provided in section 3. The directionality selection rule discussed in section 4 allows the realization of different hopping operators for the different hopping directions.

D	$U_{\mathbf{a}_1}$	$U_{\mathbf{a}_2}$	$U_{\mathbf{a}_3}$	α_x	α_y	α_z	β	Γ
1	$e^{i\phi_1\sigma_x}$			σ_x			σ_z	$i\beta\alpha_x$
2	$e^{i\phi_1\sigma_x}$	$e^{i\phi_2\sigma_y}$		σ_x	σ_y		σ_z	$i\sigma_y$
3	$e^{i\phi_1\sigma_z\otimes\sigma_x}$	$e^{i\phi_2\sigma_z\otimes\sigma_y}$	$e^{i\phi_3\sigma_z\otimes\sigma_z}$	$\sigma_z\otimes\sigma_x$	$\sigma_z\otimes\sigma_y$	$\sigma_z\otimes\sigma_z$	$\sigma_x\otimes\mathbb{I}_2$	$-i\alpha_x\alpha_y\alpha_z$

field operator, where $N_D = 2$ for one and two spatial dimensions, and $N_D = 4$ for three spatial dimensions. Our objective now is to construct an effective Hamiltonian starting from equation (2) that closely resembles the relativistic field theory in equation (12). The underlying setup consists of a gas of ultracold ^{40}K atoms, which is a non-relativistic system; nonetheless we can design it as a quantum simulator of relativistic particles by exploiting the quantum statistics and a peculiar engineerable Fermi surface.

5.1.1. Naive massless or massive Dirac fermions. The idea is to engineer translationally invariant hopping operators, $U_v = e^{i\phi_v A_v}$, according to the $\text{SU}(N_D)$ group, where N_D has been defined above. For the particular choices specified in table 4, one finds that the Hamiltonian in equation (2) in momentum space becomes

$$H = \sum_{\mathbf{k} \in \text{BZ}} \Psi_{\mathbf{k}}^\dagger \left(\sum_v 2t_v \cos \phi_v \cos k_v \mathbb{I} + 2t_v \sin \phi_v \sin k_v \alpha_v \right) \Psi_{\mathbf{k}}, \quad (13)$$

where $\Psi_{\mathbf{k}}$ is a multi-component Fermi operator that contains the different N_D hyperfine levels involved in the simulation, and \mathbf{k} is defined within the first Brillouin zone BZ. One readily observes that there are certain regimes, the so-called π -flux phases $\phi_v = \pi/2$, where the energy spectrum develops $\mathcal{N}_D = 2^D$ degeneracy points \mathbf{K}_d where the energy bands touch $\epsilon(\mathbf{K}_d) = 0$. Around these points $\mathbf{K}_d = (d_x\pi, d_y\pi, d_z\pi)$, where $d_v \in \{0, 1\}$ is a binary variable, the low-energy excitations of the ^{40}K Fermi gas are described by the effective Hamiltonian

$$H_{\text{eff}} = \sum_{\mathbf{d}} \sum_{\mathbf{p}_d} \Psi_{\mathbf{p}_d}^\dagger H_{\text{DI}}^{\mathbf{d}} \Psi(\mathbf{p}_d), \quad H_{\text{DI}}^{\mathbf{d}}(\mathbf{p}_d) = c\boldsymbol{\alpha}^{\mathbf{d}} \cdot \mathbf{p}_d, \quad (14)$$

where $\mathbf{p}_d = \mathbf{k} - \mathbf{K}_d$ represents the momentum around the degeneracy points, $(\boldsymbol{\alpha}^{\mathbf{d}})_v = (-1)^{d_v} \alpha_v$ are the Dirac matrices listed in table and $c = 2t_x = 2t_y = 2t_z$ is the Fermi velocity that plays the role of an effective speed of light. Therefore, the Fermi surface of the half-filled gas consists of a set of isolated points, the so-called Dirac points, and the low-energy excitations around those points behave according to the Hamiltonian of massless Dirac fermions in equation (14).

Let us note that we obtain an even number of relativistic-fermion species, each located around a different Dirac point (i.e. $\mathcal{N}_1 = 2$ for one dimension, $\mathcal{N}_2 = 4$ for two dimensions and

$\mathcal{N}_3 = 8$ for three dimensions). This doubling of fermionic species is a well-known phenomenon in lattice gauge theories [45], where the fermions in equation (14) would correspond to the so-called *naive Dirac fermions* [49]. As predicted by the Nielsen–Ninomiya theorem [50], this doubling cannot be avoided without breaking an underlying symmetry:

- for D odd $\{H_{\text{DI}}^{\text{d}}, \Gamma_1\} = 0$ is an involution known as chiral symmetry,
- for D even $\Gamma_2^\dagger [H_{\text{DI}}^{\text{d}}(-\mathbf{p}_{\text{d}})]^* \Gamma_2 = H_{\text{DI}}^{\text{d}}(\mathbf{p}_{\text{d}})$ is an antiunitary symmetry known as time reversal (see table 4).

According to these results, we have a quantum simulator of *massless Dirac fermions* in any spatial dimension $D = 1, 2, 3$. In $D = 1, 2$, they coincide with the *Weyl fermions*, whereas in $D = 3$ they contain a couple of Weyl fermions with opposed helicities. Note that this scheme can also be extended to simulate exotic Weyl fermions of any arbitrary spin s [51]. In addition, our quantum simulator also allows us to make these fermions massive, thus reaching the desired Hamiltonian in equation (12). The idea is to control the on-site Raman transitions such that $\Lambda = \beta$ listed in table 4. In such a case, the Rabi frequency plays the role of the mass $mc^2 = 2\Omega$, and the effective Hamiltonian in equation (14) becomes

$$H_{\text{DI}}^{\text{d}}(\mathbf{p}_{\text{d}}) = c\boldsymbol{\alpha}^{\text{d}} \cdot \mathbf{p}_{\text{d}} + mc^2\beta. \quad (15)$$

Therefore, this quantum simulator can explore both the non-relativistic and the ultra-relativistic limits of the theory.

5.1.2. The Wilson and Kaplan fermions. From a lattice gauge theory perspective, the additional fermions around $\mathbf{K}_{\text{d}} \neq \mathbf{0}$ are spurious doublers that modify the physics at long wavelengths. A partial solution is to give the doublers a very large mass $m_{\mathbf{K}_{\text{d}}}c^2$, so that they effectively decouple from the low-energy physics of the Dirac fermion at $\mathbf{K}_{\text{d}} = \mathbf{0}$, namely $m_{\mathbf{K}_{\text{d}}} \gg m_{\mathbf{K}_{\text{0}}}$. We must find a way of engineering a momentum-dependent mass that differs from the global on-site Raman mass discussed above. By combining the laser-assisted tunneling listed in table 4, with the additional terms $\tilde{U}_v = ie^{i\varphi_v\beta}$ [29], the momentum-space Hamiltonian H in equation (13) becomes $H + \tilde{H}$, where

$$\tilde{H} = \sum_{\mathbf{k} \in \text{BZ}} \Psi_{\mathbf{k}}^\dagger \left(\sum_v 2\tilde{t}_v \cos \varphi_v \sin k_v \mathbb{I} - 2\tilde{t}_v \sin \varphi_v \cos k_v \beta \right) \Psi_{\mathbf{k}}, \quad (16)$$

where \tilde{t}_v are the additional laser-assisted tunneling strengths. Once more, for the π -flux phases $\varphi_v = \pi/2$, the effective Hamiltonian in equation (12) is modified to

$$H_{\text{DI}}^{\text{d}}(\mathbf{p}_{\text{d}}) = c\boldsymbol{\alpha}^{\text{d}} \cdot \mathbf{p}_{\text{d}} + m_{\mathbf{K}_{\text{d}}}c^2\beta, \quad m_{\mathbf{K}_{\text{d}}} = m - \sum_v (-1)^{d_v} m_v, \quad (17)$$

where $m_v c^2 = 2\tilde{t}_v$. Let us emphasize that our quantum simulator provides complete control over the different masses, since m depends on the on-site Raman transition strengths, whereas m_v depends on the assisted-hopping strength and thus on the laser power. In particular, when these parameters fulfill $\sum_v m_v = m$ (i.e. $m_x = m$ for $D = 1$, $m_x + m_y = m$ for $D = 2$ and $m_x + m_y + m_z = m$ for $D = 3$), we obtain a single massless Dirac fermion at $\mathbf{K}_{\text{d}} = \mathbf{0}$, whereas the remaining doublers have been boosted to much higher energies. We thus achieve a quantum simulator of the so-called Wilson fermions of any spatial dimension $D = 1, 2, 3$ [52].

We note that this decoupling between a single massless Dirac fermion and its doublers is not in conflict with the Nielsen–Ninomiya theorem since the introduced mass terms explicitly

break the aforementioned symmetries. This is particularly important in odd dimensions, where the theory does not preserve chiral symmetry, a fundamental concept in the standard model classifying right/left-handed particles $\Gamma_1 \Psi = \pm \Psi$. To preserve such symmetries, the concept of Kaplan fermions arises [53], namely massless Dirac fermions bound to a lower-dimensional domain wall located at \mathbf{r}_\perp^* where the Wilson mass gets inverted $m_{\mathbf{K}_d} = -|m| + 2|m|\theta(\mathbf{r}_\perp - \mathbf{r}_\perp^*)$. Since we have complete experimental access to the parameters of the Wilson mass, it is also possible to tune them such that $\sum_v m_v > m$ and thus the mass $m_{\mathbf{K}_d} < 0$ gets inverted, and one gets a lower-dimensional massless fermion bound to the region where this mass inversion takes place.

Let us close this subsection by underlining the versatility of our setup as a quantum simulator of a diverse set of relativistic lattice fermions. Not only can we implement massless Dirac fermions of any dimensionality, thus exploring their connection to Weyl fermions, but also we can control their mass. This leads us to the concept of massive Dirac fermions, and the notorious Wilson and Kaplan fermions dealing with the fermion doubling problem. Interestingly enough, the physics behind these high-energy particles is intimately related to materials known as topological insulators [46], which are the subject of the following subsection. In fact, it is always possible to find a Kaplan-fermion representative within each class of topological insulators [54].

5.2. A toolbox for topological insulators

Topological insulators correspond to fermionic gapped phases of matter that are insulating in the bulk but allow robust transport along the boundaries [46]. This robustness is due to the existence of gapless edge excitations which are protected against disorder by topological arguments (i.e. they avoid Anderson localization [55] and thus transport charge even in the presence of strong disorder). The paradigmatic example of a topological insulator is the integer quantum Hall effect (IQHE) [46, 56], a 2D electron gas subjected to a strong magnetic field that displays a robust quantization of the transverse conductivity $\sigma_{xy} = n e^2/h$, where $n \in \mathbb{Z}$ is related to the topological invariant known as the Chern number [57]. In this case, chiral electrons bound to the 1D edges of the sample avoid back-scattering processes and are thus immune to disorder [58]. Remarkably enough, the IQHE is only one instance of a large list of topological insulating phases. Each class can be characterized by a set of discrete fundamental symmetries [59] and a certain topological invariant; see table 5. Note that we have excluded the topological superfluids from this table, since their quantum simulation would require a pairing mechanism and thus goes beyond the scope of this work [60, 61]. We now discuss how our quantum simulator can reproduce the properties of many of these fascinating phases of matter following two possible strategies.

5.2.1. Bottom-up approach. In this case, one designs the ultracold-atom Hamiltonian so that it simulates a particular model belonging to the desired class of topological insulators. Therefore, a different experiment would be required for each class-oriented simulator. Two representative, yet reasonably simple examples are the Su–Schrieffer–Hegger model of polyacetylene [62], which is related to the $D = 1$ BDI topological insulator or the π -flux phase of the fermionic Creutz ladder [63], which is related to the $D = 1$ AIII topological insulator. The former can be simulated by using a one-component Fermi gas in a 1D dimerized optical superlattice, thus

Table 5. Periodic table of topological insulators. The underlying quadratic Hamiltonians $H = \sum_{\alpha\beta} \Psi_{\alpha}^{\dagger} \mathbb{H}_{\alpha\beta} \Psi_{\beta} + \text{h.c.}$, where α, β represent the lattice sites and the internal states of the fermion, can be classified according to the fundamental symmetries of time-reversal \mathcal{T} , charge conjugation \mathcal{C} and a combination of both $\mathcal{S} = \mathcal{TC}$. The values $T = 0, C = 0, S = 0$ are assigned to Hamiltonians that break the symmetry, whereas $T = \pm 1, C = \pm 1, S = 1$ correspond to symmetry-preserving Hamiltonians, where $\mathcal{T}^2 = \pm 1, \mathcal{C}^2 = \pm 1, \mathcal{S}^2 = +1$. There are six possible combinations for non-interacting fermionic Hamiltonians (and another four for pairing fermionic Hamiltonians), which lead to the classes listed in the first column. For each dimension d , there are three possible topological insulators among all these classes, and they are classified according to the integer \mathbb{Z} or binary \mathbb{Z}_2 nature of a certain topological invariant. In the column labeled QS, we list the particular instances that can be simulated with our superlattice-based quantum simulator.

Class	Name	T	C	S	$d = 1$	QS	$d = 2$	QS	$d = 3$	QS
A	Unitary	0	0	0	0		\mathbb{Z}	Yes	0	
AIII	Chiral unitary	0	0	1	\mathbb{Z}	Yes	0		\mathbb{Z}	Yes
AI	Orthogonal	+1	0	0	0		0		0	
BDI	Chiral orthogonal	+1	+1	1	\mathbb{Z}	?	0		0	
AII	Symplectic	-1	0	0	0		\mathbb{Z}_2	Yes	\mathbb{Z}_2	Yes
CII	Chiral symplectic	-1	-1	1	$2\mathbb{Z}$	Yes	0		\mathbb{Z}_2	Yes

obtaining

$$H_{\text{BDI}} = \sum_n (t - \delta) c_{2n-1}^{\dagger} c_{2n} + (t + \delta) c_{2n}^{\dagger} c_{2n-1} + \text{h.c.}, \quad (18)$$

where δ quantifies the different tunneling strengths between superlattice sites [36]. On the other hand, the Creutz ladder is described by

$$H_{\text{AIII}} = \sum_n K e^{-i\theta} a_{n+1}^{\dagger} a_n + K e^{i\theta} b_{n+1}^{\dagger} b_n + K b_{n+1}^{\dagger} a_n + K a_{n+1}^{\dagger} b_n + M a_n^{\dagger} b_n + \text{h.c.}, \quad (19)$$

where K, M are tunneling strengths and θ is a magnetic flux piercing the ladder. This requires two Zeeman sublevels to be assigned to the fermion species a_n, b_n and a 1D laser-assisted tunneling $U_{a_1} = \text{diag}\{e^{-i\theta}, e^{i\theta}\}$, $\tilde{U}_{a_1} = i\sigma_x$, together with the Raman on-site operator of strength M [64].

It is possible to continue this approach, proceeding thus to higher dimensions and different topological classes. Prominent examples would be the honeycomb time-reversal breaking Haldane model [65, 66] for the $D = 2$ topological insulator in class A or the time-reversal Kane–Mele model in the honeycomb lattice in class AII [67] or other optical-lattice geometries [26, 68, 69]. Rather than following this route, we shall explore a different approach that is better suited to the superlattice-based simulator introduced above. Indeed, we shall argue that this quantum simulator allows the reproduction of most of the topological phases in table.

5.2.2. Dimensional-reduction approach. In this case, the starting point is the quantum simulator of D -dimensional Kaplan fermions in equation (17). Depending on the particular

Table 6. Quantum simulator of topological insulators. We list different realizations of Wilson-fermion Hamiltonians in equation (20) that directly lead to several classes of topological insulators. Each class, characterized by the discrete symmetries $\mathcal{T}, \mathcal{C}, \mathcal{S}$, where $\mathcal{T}^2 = \Theta_T \Theta_T^* = \pm 1$ and $\mathcal{C}^2 = \Theta_C \Theta_C^* = \pm 1$. In addition, each class has a Wilson-fermion representative with a particular choice of the Clifford algebra α_ν, β that depends on the dimensionality D and the corresponding symmetries. We also highlight the topological insulators that can be obtained by dimensional reduction from a parent Hamiltonian, such as AII, $D = 3 \hookrightarrow$ AII, $D = 2$, or A, $D = 2 \hookrightarrow$ AIII, $D = 1$. We also list the unitary matrices Θ_T, Θ_C involved in the definition of the discrete symmetries.

Class	D	α_x	α_y	α_z	β	Θ_T	Θ_C	\mathcal{T}	\mathcal{C}	\mathcal{S}
CII	3	$\sigma_z \otimes \sigma_x$	$\sigma_z \otimes \sigma_y$	$\sigma_z \otimes \sigma_z$	$\sigma_z \otimes \mathbb{I}_2$	$i\mathbb{I} \otimes \sigma_y$	$i\sigma_x \otimes \sigma_y$	-1	-1	1
AIII	3	$\sigma_z \otimes \sigma_x$	$\sigma_z \otimes \sigma_y$	$\sigma_z \otimes \sigma_z$	$\sigma_y \otimes \mathbb{I}_2$	$i\mathbb{I} \otimes \sigma_y$	$i\sigma_x \otimes \sigma_y$	0	0	1
AII	3	$\sigma_z \otimes \sigma_x$	$\sigma_z \otimes \sigma_y$	$\sigma_z \otimes \sigma_z$	$\sigma_x \otimes \mathbb{I}_2$	$i\mathbb{I} \otimes \sigma_y$	$i\sigma_x \otimes \sigma_y$	-1	0	0
\hookrightarrow AII	2	$\sigma_z \otimes \sigma_x$	$\sigma_z \otimes \sigma_y$		$\sigma_x \otimes \mathbb{I}_2$	$i\mathbb{I} \otimes \sigma_y$	$i\sigma_x \otimes \sigma_y$	-1	0	0
A	2	σ_x	σ_y		σ_z	\mathbb{I}	$i\sigma_x$	0	0	0
\hookrightarrow AIII	1	σ_x			σ_z	\mathbb{I}	$i\sigma_x$	0	0	1
CII	1	$\sigma_z \otimes \sigma_x$			$\sigma_z \otimes \mathbb{I}_2$	$i\mathbb{I} \otimes \sigma_y$	$i\sigma_x \otimes \sigma_y$	-1	-1	1

choice of Dirac matrices, the inverted-mass regime will correspond to a different class of topological insulators. In addition, in some situations, a dimensional reduction [54] that amounts to an increase of the optical-lattice depth in one direction, connects us to a different lower-dimensional class. We rewrite the full Hamiltonian

$$H_{\text{eff}} = \sum_{\mathbf{d}, \mathbf{p}_d} \Psi^\dagger(\mathbf{p}_d) H_{\text{DI}}^{\mathbf{d}} \Psi(\mathbf{p}_d), \quad H_{\text{DI}}^{\mathbf{d}}(\mathbf{p}_d) = c\alpha^{\mathbf{d}} \cdot \mathbf{p}_d + m_{\mathbf{K}_d} c^2 \beta, \quad (20)$$

where the Wilson mass is $m_{\mathbf{K}_d} = m - \sum_\nu (-1)^{d_\nu} m_\nu$ and where the Dirac matrices $\alpha_\nu^{\mathbf{d}}, \beta$ will be selected so that the $\mathcal{T}, \mathcal{C}, \mathcal{S}$ symmetries are explicitly broken or preserved. This translationally invariant Hamiltonian preserves these symmetries when the following conditions are met:

$$\mathcal{T}: \quad \Theta_T^\dagger [H_{\text{DI}}^{\mathbf{d}}(-\mathbf{p}_d)]^* \Theta_T = +H_{\text{DI}}^{\mathbf{d}}(\mathbf{p}_d), \quad (21)$$

$$\mathcal{C}: \quad \Theta_C^\dagger [H_{\text{DI}}^{\mathbf{d}}(-\mathbf{p}_d)]^* \Theta_C = -H_{\text{DI}}^{\mathbf{d}}(\mathbf{p}_d), \quad (22)$$

$$\mathcal{S}: \quad \left[\Theta_T^\dagger \right]^* \Theta_C^\dagger H_{\text{DI}}^{\mathbf{d}}(\mathbf{p}_d) \Theta_C \Theta_T^* = -H_{\text{DI}}^{\mathbf{d}}(\mathbf{p}_d), \quad (23)$$

where Θ_T, Θ_C are some unitary matrices. In table 6, we list the symmetry properties of different Kaplan-fermion Hamiltonians. It is important to note that these symmetries might correspond to the exact symmetries in nature (e.g. when considering the hyperfine levels $\{|F, m_F\rangle, |F, -m_F\rangle\}$, the time-reversal symmetry given by $\theta_T = i\sigma_y$ exactly corresponds to time-reversal symmetry in nature). Conversely, these symmetries might otherwise correspond to the algebraic properties of the effective Hamiltonian. Let us emphasize, however, that as far as the disorder respects such symmetries, the robustness of the edge excitations is guaranteed. It would be of the greatest interest to design disorder breaking or preserving such symmetries, generalizing the studies on Anderson localization [6, 7].

In table 6, we have listed the different topological insulators that can be simulated with our scheme. As shown in [29] for the particular case of 3D AII insulators, the laser parameters can be controlled so that an *odd* number of Wilson masses are inverted. This mass inversion occurs through a gap-closing point and thus a quantum phase transition between a normal band insulator and a topological one occurs. This new phase is characterized by an *odd* number of massless fermionic excitations (i.e. massless Dirac fermions) bound to the boundaries of the system, and protected by a topological invariant. In the 3D case, this corresponds to an axion term that modifies the response of the system according to the so-called axion electrodynamics [70]. Remarkably, table 6 contains all of the relevant information to explore the exotic properties of different topological insulators in a superlattice-based experiment with ultracold atoms.

6. Conclusions

In this paper, we have presented a concrete proposal for the realization of laser-assisted tunneling in a spin-independent optical lattice trapping a multi-spin atomic gas. Remarkably enough, it is possible to tailor a wide range of spin-flipping hopping operators, which opens an interesting route to push the experiments beyond the standard superfluid–Mott insulator transition. The scheme we have presented combines bi-chromatic lattices and Raman transfers, to adiabatically eliminate the states trapped in the middle of each lattice link. These states act as simple spectators that assist the tunneling of atoms between the main minima of the optical lattice. This mechanism is clearly supported by our numerical simulations of the time evolution of the atomic population between the different optical-lattice sites. Even though we focus on fermionic ^{40}K , we stress that the ingredients of this proposal do not rely on the atomic statistics and could thus be used for all the alkalis.

We believe that such a device could have important applications in the quantum simulation of non-interacting lattice field theories, which are characterized, in their discrete version, by on-site and nearest-neighbor hopping Hamiltonians. Once the fields of the theory to be simulated are mapped into the atomic hyperfine states, the desired operators correspond to population transfers between such levels. The former can be realized by standard microwaves, whereas the latter might be tailored with the laser-assisted schemes described here.

Even though interactions are at the heart of a plethora of interesting effects, non-interacting fermionic theories already encompass a number of phenomena whose experimental realization would be of the greatest interest. In the second part of the paper, we analyzed interesting physical models that could benefit from our proposal. In particular, we focused on relativistic field theories and showed that there is a zoo of relativistic lattice fermions that can be addressed with this platform. In addition, we presented a toolbox to design particular assisted tunneling processes that lead us to the physics of topological insulators. Remarkably enough, this quantum simulator turns out to be extremely versatile, since most of the phases of the periodic table of topological insulators can be addressed.

Finally, let us comment on the possible combination of this proposal with the control of interactions already achieved in cold-atom gases. This might eventually boost experiments into regimes where classical numerical simulations fail, which we leave as an outlook for future work. In particular, the problem of robustness of topological orders (classified for non-interacting theories) with respect to interactions is one of the most important challenges of the

modern condensed matter [71]. We believe that a direct combination of our setup with Feshbach resonances will provide important insights into this unsolved question.

Acknowledgments

LM and MR acknowledge fruitful discussions with U Schneider with whom the superlattice idea was actually conceived. We also thank J I Cirac, S Dürr, G Juzeliunas, W Phillips, I Spielman, and C Wu. LM and MR thank Caixa Manresa and ICFO for hospitality; MR and ML thank KITP for hospitality. MR and ML have received funding from the European Community's Seventh Framework Programme (FP7/2007-2013) under grant agreement no. 247687 (IP-AQUTE). ML also acknowledges financial support from ERC Grant QUAGATUA, EU STREP NAMEQUAM, MINCIN FIS2008-00784, the Alexander von Humboldt Foundation and Hamburg Theory Award. NG thanks the FRS-FNRS for financial support. AB and MAMD thank MICINN FIS2009-10061, CAM QUITEMAD, European FET-7 PICC and UCM-BS GICC-910758.

References

- [1] Feynman R P 1982 *Int. J. Theor. Phys.* **21** 467
- [2] Lloyd S 1996 *Science* **273** 1073
- [3] Buluta I and Nori F 2009 *Science* **326** 5949
- [4] Bloch I, Dalibard J and Zwerger W 2008 *Rev. Mod. Phys.* **80** 885
- [5] Lewenstein A, Sanpera A, Ahufinger V, Damski B, Sen A and Sen U 2007 *Adv. Phys.* **56** 243
- [6] Billy J, Josse V, Bernard A, Hambrecht Lugan P, Clément D, Sanchez-Palencia L, Bouyer P and Aspect A 2008 *Nature* **453** 891
- [7] Giacomo R, D'Errico C, Fallani L, Fattori M, Fort C, Zaccanti M, Modugno G, Modugno M and Inguscio M 2008 *Nature* **453** 895
- [8] Jo G-B, Lee Y-R, Choi J-H, Christensen C A, Kim T H, Thywissen J H, Pritchard D E and Ketterle W 2009 *Science* **325** 1521
- [9] Nascimbène S, Navon N, Jiang K J, Chevy F and Salomon C 2010 *Nature* **463** 1050
- [10] Ezawa Z 2000 *Quantum Hall Effects: Field Theoretical Approach and Related Topics* (Singapore: World Scientific)
- [11] Dalibard J, Gerbier F, Juzeliūnas J and Öhberg P 2011 *Rev. Mod. Phys.* **83** 1523
- [12] Lin Y-J, Compton R L, Jiménez-García K, Porto J V and Spielman I B 2009 *Nature* **462** 628
- [13] Lin Y-J, Compton R L, Jiménez-García K, Phillips W D, Porto J V and Spielman I B 2011 *Nat. Phys.* **7** 531
- [14] Lin Y-J, Jiménez-García K and Spielman I B 2011 *Nature* **471** 83
- [15] Jaksch D and Zoller P 2003 *New J. Phys.* **5** 56
- [16] Gerbier F and Dalibard J 2010 *New J. Phys.* **12** 033007
- [17] Osterloh K, Baig M, Santos L, Zoller P and Lewenstein M 2005 *Phys. Rev. Lett.* **95** 010403
- [18] Goldman N, Kubasiak A, Gaspard P and Lewenstein M 2009 *Phys. Rev. A* **79** 023624
- [19] Sørensen A S, Demler E and Lukin M D 2005 *Phys. Rev. Lett.* **94** 086803
- [20] Hafezi M, Sørensen A S, Demler E and Lukin M D 2007 *Phys. Rev. A* **76** 023613
- [21] Palmer R, Klein A and Jaksch D 2008 *Phys. Rev. A* **78** 013609
- [22] Möller G and Cooper N 2009 *Phys. Rev. Lett.* **103** 105303
- [23] Umucalilar R O and Mueller E J 2010 *Phys. Rev. A* **81** 053628
- [24] Goldman N, Kubasiak A, Bermudez A, Gaspard P, Lewenstein M and Martin-Delgado M A 2009 *Phys. Rev. Lett.* **103** 035301

- [25] Liu X-J, Liu X, Wu C and Sinova J 2010 *Phys. Rev. A* **81** 033622
- [26] Goldman N, Satija I, Nikolic P, Bermudez A, Martin-Delgado M A, Lewenstein M and Spielman I B 2010 *Phys. Rev. Lett.* **105** 255302
- [27] Stanescu T D, Galitski V and Das Sarma S 2010 *Phys. Rev. A* **82** 013608
- [28] Cooper N R 2011 *Phys. Rev. Lett.* **106** 175301
Béri B and Cooper N R 2011 *Phys. Rev. Lett.* **107** 145301
- [29] Bermudez A, Mazza L, Rizzi M, Goldman N, Lewenstein M and Martin-Delgado M A 2010 *Phys. Rev. Lett.* **105** 190404
- [30] Tang E, Mei J-W and Wen X-G 2011 *Phys. Rev. Lett.* **106** 236802
Sun K, Gu Z, Katsura H and Das Sarma A 2011 *Phys. Rev. Lett.* **106** 236803
Neupert T, Santos L, Chamon C and Mudry C 2011 *Phys. Rev. Lett.* **106** 236804
- [31] Heikkilä T T, Kopnin N B and Volovik G E 2011 *Pis'ma Zh. Eksp. Teor. Fiz.* **94** 252 (arXiv:1012.0905)
Kopnin N B, Heikkilä T T and Volovik G E 2011 *Phys. Rev. B* **83** 220503(R) (arXiv:1103.2033)
Heikkilä T T and Volovik G E 2011 *JETP Lett.* **93** 59 (arXiv:1011.4185)
Volovik G E 2011 *JETP Lett.* **93** 66 (arXiv:1011.4665)
- [32] Burrello M and Trombettoni A 2010 *Phys. Rev. Lett.* **105** 125304
- [33] Hou J-M, Yang W-X and Liu X-J 2009 *Phys. Rev. A* **79** 043621
- [34] Lim L-K, Lazarides A, Hemmerich A and Morais Smith C 2009 *Europhys. Lett.* **88** 36001
- [35] Lepori L, Mussardo G and Trombettoni A 2010 *Europhys. Lett.* **92** 50003
- [36] Cirac J I, Maraner P and Pachos J K 2010 *Phys. Rev. Lett.* **105** 190403
- [37] Boada O, Celi A, Latorre J I and Lewenstein M 2010 *New J. Phys.* **13** 035002
- [38] Zhu S-L, Wang B and Duan L-M 2007 *Phys. Rev. Lett.* **98** 260402
Lee K L, Gremaud B, Han R, Englert B-G and Miniatura C 2009 *Phys. Rev. A* **80** 043411
Bermudez A, Goldman N, Kubasiak A, Lewenstein M and Martin-Delgado M A 2010 *New J. Phys.* **12** 033041
- [39] Witthaut D, Salger T, Kling S, Grossert C and Weitz M 2011 *Phys. Rev. A* **84** 033601 (arXiv:1102.4047)
- [40] Szpak N and Schützold R 2011 *Phys. Rev. A* **84** 050101(R) (arXiv:1103.0541)
- [41] Mazza L, Rizzi M, Lewenstein M and Cirac J I 2010 *Phys. Rev. A* **82** 043629
- [42] Jaksch D, Bruder C, Cirac J I, Gardiner C W and Zoller P 1998 *Phys. Rev. Lett.* **81** 3108
- [43] Köhl M, Moritz H, Stöferle T, Günter K and Esslinger T 2005 *Phys. Rev. Lett.* **94** 080403
- [44] Kohn W 1959 *Phys. Rev.* **115** 809
- [45] Kogut J B 1983 *Rev. Mod. Phys.* **55** 775
- [46] Hasan M Z and Kane C L 2010 *Rev. Mod. Phys.* **82** 3045
Qi X-L and Zhang S-C 2011 *Rev. Mod. Phys.* **83** 1057
- [47] Castro Neto A H, Guinea F, Peres N M R, Novoselov K S and Geim A K 2009 *Rev. Mod. Phys.* **81** 109
- [48] Peskin M E and Schroeder D V 1995 *An Introduction to Quantum Field Theory* (Boulder, CO: Westview Press)
- [49] Karsten L-H and Smit J 1981 *Nucl. Phys. B* **183** 103
- [50] Nielsen H B and Ninomiya M 1980 *Nucl. Phys. B* **185** 20
Nielsen H B and Ninomiya M 1981 *Nucl. Phys. B* **193** 173
- [51] Lan Z, Goldman N, Bermudez A, Lu W and Ohberg P 2011 *Phys. Rev. B* **84** 165115
- [52] Wilson K 1977 *New Phenomena in Subnuclear Physics* ed A Zichichi (New York: Plenum) p 69
- [53] Kaplan D B 1992 *Phys. Lett. B* **288** 342
- [54] Qi X-L, Hughes T L and Zhang S-C 2008 *Phys. Rev. B* **78** 195424
Ryu S, Schnyder A P, Furusaki A and Ludwig A W W 2010 *New J. Phys.* **12** 065010
- [55] Anderson P W 1958 *Phys. Rev.* **109** 1492
- [56] von Klitzing K 1986 *Rev. Mod. Phys.* **58** 519
- [57] Thouless D J, Kohmoto M, Nightingale M P and den Nijs M *Phys. Rev. Lett.* **49** 405
- [58] Halperin B I 1982 *Phys. Rev. B* **25** 2185

- [59] Schnyder A P, Ryu S, Furusaki A and Ludwig A W W 2008 *Phys. Rev. B* **78** 195125
Kitaev A Y 2009 *AIP Conf. Proc.* **1134** 22
- [60] Sato M, Takahashi Y and Fujimoto S 2009 *Phys. Rev. Lett.* **103** 020401
Kubasiak A, Massignan P and Lewenstein M 2010 *Europhys. Lett.* **92** 46004
- [61] Zhu S-L, Shao L-B, Wang Z D and Duan L-M 2011 *Phys. Rev. Lett.* **106** 100404
- [62] Su W P, Schrieffer J R and Heeger A J 1979 *Phys. Rev. Lett.* **42** 1698
- [63] Creutz M 1999 *Phys. Rev. Lett.* **83** 2636
- [64] Bermudez A, Patane D, Amico L and Martin-Delgado M A 2009 *Phys. Rev. Lett.* **102** 135702
- [65] Haldane F D M 1988 *Phys. Rev. Lett.* **61** 2015
- [66] Shao L B, Zhu S-L, Sheng L, Xing D Y and Wang Z D 2008 *Phys. Rev. Lett.* **101** 246810
Stanescu T D, Galitski V and Das Sarma S 2010 *Phys. Rev. A* **82** 013608
Liu X-J, Liu X, Wu C and Sinova J 2010 *Phys. Rev. A* **81** 033622
- [67] Kane C L and Mele E J 2005 *Phys. Rev. Lett.* **95** 226801
- [68] Liu G, Zhu S-L, Jiang S, Sun F and Liu W M 2010 *Phys. Rev. A* **82** 053605
- [69] Goldman N, Urban D F and Bercioux D 2011 *Phys. Rev. A* **83** 063601
- [70] Wilczek F 1987 *Phys. Rev. Lett.* **58** 1799
Qi X-L, Li R, Zang J and Zhang S-C 2009 *Science* **323** 1184
- [71] Heikkila T T and Volovik G E 2010 *JETP Lett.* **92** 681
Wang Z, Qi X L and Zhang S C 2010 *Phys. Rev. Lett.* **105** 256803
Ryu S and Takayanagi T 2010 *Phys. Rev. D* **82** 086014
Kou S P and Wen X G 2010 *Phys. Rev. B* **82** 144501
Ryu S, Schnyder A P, Furusaki A and Ludwig A W W 2010 *New J. Phys.* **12** 065010
Fidkowski L and Kitaev A 2011 *Phys. Rev. B* **83** 075103
Turner A M, Pollmann F and Berg E 2011 *Phys. Rev. B* **83** 075102
Xie C, Gu Z-C and Wen X-G 2011 *Phys. Rev. B* **83** 035107
Gurarie V 2011 *Phys. Rev. B* **83** 085426